JACS
JOURNAL OF THE AMERICAN CHEMICAL SOCIETY
Article
pubs.acs.org/JACS

Thermal Methane Conversion to Syngas Mediated by Rh_1-Doped Aluminum Oxide Cluster Cations $RhAl_3O_4^+$

Ya-Ke Li,[†,§] Zhen Yuan,[†,§] Yan-Xia Zhao,[*,†] Chongyang Zhao,[‡,§] Qing-Yu Liu,[†,§] Hui Chen,[*,‡] and Sheng-Gui He[*,†]

[†]Beijing National Laboratory for Molecular Sciences, State Key Laboratory for Structural Chemistry of Unstable and Stable Species, Institute of Chemistry, Chinese Academy of Sciences, Beijing 100190, P. R. China

[‡]Beijing National Laboratory for Molecular Sciences, Key Laboratory of Photochemistry, Institute of Chemistry, Chinese Academy of Sciences, Beijing 100190, P. R. China

[§]University of Chinese Academy of Sciences, Beijing 100049, P. R. China

Supporting Information

ABSTRACT: Laser ablation generated $RhAl_3O_4^+$ heteronuclear metal oxide cluster cations have been mass-selected using a quadrupole mass filter and reacted with CH_4 or CD_4 in a linear ion trap reactor under thermal collision conditions. The reactions have been characterized by state-of-the-art mass spectrometry and quantum chemistry calculations. The $RhAl_3O_4^+$ cluster can activate four C−H bonds of a methane molecule and convert methane to syngas, an important intermediate product in methane conversion to value-added chemicals. The Rh atom is the active site for activation of the C−H bonds of methane. The high electron-withdrawing capability of Rh atom is the driving force to promote the conversion of methane to syngas. The polarity of Rh oxidation state is changed from positive to negative after the reaction. This study has provided the first example of methane conversion to syngas by heteronuclear metal oxide clusters under thermal collision conditions. Furthermore, the molecular level origin has been revealed for the condensed-phase experimental observation that trace amounts of Rh can promote the participation of lattice oxygen of chemically very inert support (Al_2O_3) to oxidize methane to carbon monoxide.

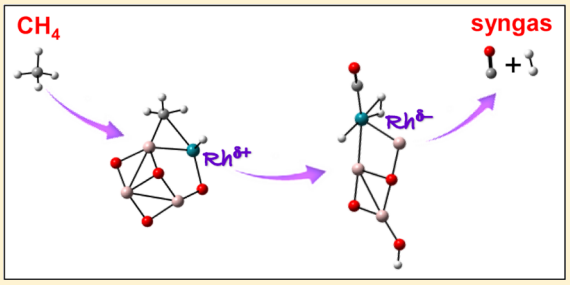

1. INTRODUCTION

Production of syngas has been extensively explored in order to provide raw materials for industrially important reactions such as Fischer−Tropsch and methanol synthesis.[1,2] Conversion of methane, the primary constituent of natural gas, is one of the main ways to produce syngas.[2] Much research effort has been devoted to the development of catalysts with high activity and selectivity for the conversion of methane to syngas. Rhodium catalysts supported on aluminum oxides have been reported to exhibit excellent performance.[3] Furthermore, higher activity and selectivity were identified for the smaller Rh nanoparticles than the bigger ones.[3b,4] It has been reported that trace amounts of Rh can promote the direct participation of lattice oxygen of chemically very inert supports such as aluminum oxide (Al_2O_3) to oxidize methane to carbon monoxide.[3b,c,5] However, due to the complexity of condensed-phase system, the function of the Rh atoms and the mechanistic details in the reactions of methane with the Rh/Al_2O_3 catalysts at a molecular level remain unclear. Study of gas-phase atomic clusters under isolated, controlled, and reproducible conditions provides an important way to uncover the mechanistic details in related condensed-phase reactions at a molecular level.[6]

The reactions of methane with rhodium species,[7] bare rhodium clusters $Rh_n^{+/0}$,[8] and aluminum oxide clusters $Al_xO_y^+$[9] have been studied by mass spectrometric experiments or theoretical calculations. The independent roles of rhodium atoms and atomic oxygen radical anions ($O^{-\bullet}$) played in C−H bond activation of methane have been identified. However, at most two C−H bonds of a methane molecule were activated in those reported reaction systems,[7−9] so no syngas was produced. To have a better understanding of the molecular level mechanisms, the nature of Rh species, and the roles of alumina support in syngas production over realistic Rh/Al_2O_3 catalysts, it is quite necessary to study the reactions between methane and the composite systems with both the Rh atoms and the aluminum oxide clusters.

In this work, the rhodium−aluminum (Rh−Al) heteronuclear oxide cluster cations $Rh_xAl_yO_z^+$ were prepared and reacted with methane in an ion trap reactor under mild conditions. Among the many prepared Rh−Al oxide cluster cations, the $RhAl_3O_4^+$ cluster was highly reactive toward methane and the syngas was generated. This study has provided the first example of methane conversion to syngas by Rh−Al heteronuclear oxide cluster cations.

Received: May 27, 2016
Published: September 8, 2016

DOI: 10.1021/jacs.6b05454
J. Am. Chem. Soc. 2016, 138, 12854−12860

2. METHODS

Experimental Method. Details of the experimental setup can be found in our previous studies,[10] and only a brief outline of the experiments is given below. The $Rh_xAl_y{}^{18}O_z{}^+$ clusters were generated by laser ablation of a mixed metal disk compressed with Rh and Al powders (molar ratio: Rh/Al = 1/1) in the presence of 0.01% $^{18}O_2$ seeded in a He carrier gas with the backing pressure of 6.0 standard atmospheres. It is noteworthy that when $^{16}O_2$ was used as oxygen source to generate the clusters it was difficult to mass-select $RhAl_3{}^{16}O_4{}^+$ (m/z = 248) from $Al_5{}^{16}O_7{}^+$ (m/z = 247) and $Rh_2Al^{16}O^+$ (m/z = 249) because the relative intensity of the generated $RhAl_3{}^{16}O_4{}^+$ cluster was very weak. The cluster ions of interest were mass-selected by a quadrupole mass filter (QMF)[10b] and entered into a linear ion trap (LIT)[10a] reactor, where they were confined and thermalized (Figure S1) by collisions with a pulse of He gas for about 2.6 ms. The thermalized ions then interacted with a pulse of CH_4 or CD_4 for around 1.5 ms. The instantaneous gas pressure of He in the reactor was around 1 Pa (~800 collisions) and longer cooling time (>2.6 ms) did not affect the reaction efficiency, indicating that the $RhAl_3O_4{}^+$ ions had been thermalized before they reacted with methane. The partial pressures of the reactant molecules ranged from about 2 mPa (1 mPa = 10^{-3} Pa) to more than 60 mPa. The temperature of the cooling gas (He), the reactant gases (CH_4 and CD_4), and the LIT reactor was around 298 K. The LIT was formed by a set of hexapole rods and two cap electrodes. A reflectron time-of-flight (TOF) mass spectrometer[10c] was used to measure masses and abundances of the reactant and product ions.

Theoretical Method. Density functional theory (DFT) calculations using Gaussian 09 program[11] were carried out to investigate the structures of $RhAl_3O_4{}^+$ and the mechanisms of reaction with CH_4. The B3P86 functional[12] was tested (Table S1) and adopted. The reaction mechanism calculations involved geometry optimizations of reaction intermediates and transition states (TSs). The initial guess structures of the TS species were obtained through relaxed potential energy surface scans using single or multiple internal coordinates.[13] Vibrational frequency calculations were performed to check that each of the intermediates and TSs has zero and only one imaginary frequency, respectively. The intrinsic reaction coordinate calculations[14] were carried out to make sure that a TS connects two appropriate minima. The reported energies (ΔH_0) were corrected with zero-point vibrations. The natural bond orbital (NBO) analysis was performed with NBO 3.1.[15]

To determine more reliable relative energies of products P1 ($RhAl_3O_4CH_2{}^+ + H_2$) and P2 ($RhAl_3O_3H_4{}^+ + CO$), the single-point energy calculations at the DFT optimized structures were carried out employing partially spin-adapted explicitly correlated RCCSD(T)-F12 method [RCCSD(T) = restricted coupled-cluster method with single, double, and perturbative triple excitations]. The Molpro program package was used in RCCSD(T)-F12 calculations[16] in which the details were given in the Supporting Information.

The Rice–Ramsperger–Kassel–Marcus (RRKM) theory and RRKM-based variational TS theory (VTST)[17] were used to calculate the rate constants of traversing TSs from intermediates, desorption of CH_4 from the encounter complex, and desorption of H_2 and CO from one of the reaction intermediates. For these calculations, the energy (E) of the reaction intermediate and the energy barrier ($E^{\ddagger}$) for each step were needed. The reaction intermediate possesses the vibrational energies (E_{vib}) of $RhAl_3O_4{}^+$ and CH_4/CD_4, the center of mass kinetic energy (E_k), and the binding energy (E_b) which is the energy difference between the separated reactants ($RhAl_3O_4{}^+ + CH_4/CD_4$) and the reaction complex. The values of E_{vib} and E_b were taken from the DFT calculations and $E_k = \mu v^2/2$, in which μ is the reduced mass and v is the velocity (≈680 m/s). The VTST calculations involved geometry optimizations of $RhAl_3O_iC_jH_kX^+$ [X = CH_4 (i = 4, j = 0, k = 0), H_2 (i = 4, j = 1, k = 2), or CO (i = 3, j = 0, k = 4)] by fixing the distance between $RhAl_3O_iC_jH_k$ and the X moiety at various values. The densities and the numbers of states required for RRKM and VTST calculations were obtained by the direct count method[18] with the DFT calculated vibrational frequencies under the approximation of harmonic vibrations.

3. RESULTS AND DISCUSSION

The TOF mass spectra for the interactions of laser ablation generated, mass-selected, and thermalized $RhAl_3{}^{18}O_4{}^+$ (m/z = 256) cluster cations with CH_4 and CD_4 are shown in Figure 1.

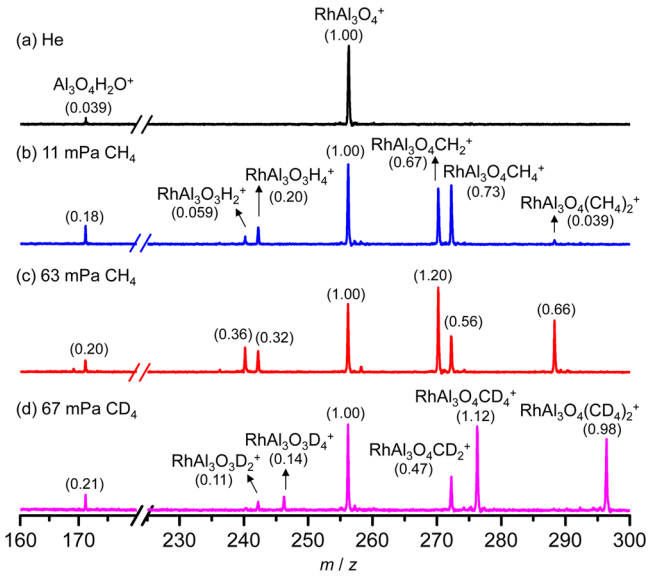

Figure 1. TOF mass spectra for the reactions of mass-selected $RhAl_3O_4{}^+$ with (a) He, (b) 11 mPa CH_4, (c) 63 mPa CH_4, and (d) 67 mPa CD_4. The reaction time is about 1.5 ms. The values in the parentheses are the relative peak intensities in each panel. The appearance of $Al_3O_4H_2O^+$ in panels (a)–(d) is due to the reaction with water impurity ($RhAl_3O_4{}^+ + H_2O \rightarrow Al_3O_4H_2O^+ + Rh$) during confining and cooling the cluster ions. The ratios of $Al_3O_4H_2O^+$ intensity to the total ion intensities in panels (a)–(d) are almost the same (5 ± 1)%.

Upon interaction of $RhAl_3O_4{}^+$ with 11 mPa CH_4 for 1.5 ms (Figure 1b), in addition to the association complex $RhAl_3O_4CH_4{}^+$ (P3), the products $RhAl_3O_4CH_2{}^+$ (P1), $RhAl_3O_3H_4{}^+$ (P2), $RhAl_3O_3H_2{}^+$, and $RhAl_3O_4(CH_4)_2{}^+$ were observed. The secondary product $RhAl_3O_4(CH_4)_2{}^+$ became relatively strong under a high CH_4 pressure (63 mPa, Figure 1c). The $RhAl_3O_3H_2{}^+$ peak was weaker than $RhAl_3O_3H_4{}^+$ under low CH_4 pressure (Figure 1b) while $RhAl_3O_3H_2{}^+$ became stronger than $RhAl_3O_3H_4{}^+$ under high CH_4 pressure (Figure 1c), indicating that $RhAl_3O_3H_2{}^+$ was also due to the secondary reaction. The intensity ratios of $RhAl_3O_3H_4{}^+$ to $RhAl_3O_4CH_2{}^+$ in Figure 1b and c are the same (0.28 ± 0.02) within the experimental uncertainties (±10%) so both of them can be due to the primary reactions:

$$RhAl_3O_4{}^+ + CH_4 \rightarrow RhAl_3O_4CH_2{}^+ + H_2 \quad (1)$$

$$RhAl_3O_4{}^+ + CH_4 \rightarrow RhAl_3O_3H_4{}^+ + CO \quad (2)$$

The assignments of the products in Figure 1b were further confirmed in the isotopic labeling experiment with CD_4 (Figure 1d). It is noticeable that the adopted experimental setup was not able to identify the neutral products H_2 and CO. Additional experimental techniques such as multiphoton ionization with pulsed lasers are required to observe these neutral molecules.[19]

DOI: 10.1021/jacs.6b05454
J. Am. Chem. Soc. 2016, 138, 12854–12860

The number of the $RhAl_3O_4^+$ cluster ions was far less than that of the CH_4 molecules in the ion trap reactor so the pseudo-first-order kinetics was assumed for the bimolecular reaction between $RhAl_3O_4^+$ and CH_4.[10a,20] The total rate constants (k_1), which correspond to relative signal depletion of the reactant cluster ions ($RhAl_3O_4^+$) with respect to the pressure increase of methane molecules, amount to 7.4×10^{-10} and 4.3×10^{-10} cm^3 $molecule^{-1}$ s^{-1} for the reactions of $RhAl_3O_4^+$ with CH_4 and CD_4, respectively. The kinetic isotope effect [KIE = $k_1(RhAl_3O_4^+ + CH_4)/ k_1(RhAl_3O_4^+ + CD_4)$] was estimated to be 1.7. The theoretical collision rate constant[21] [$k_{coll} = 2\pi(e^2\alpha/\mu)^{1/2}$, in which e is the charge of the cluster ion, α is the electric polarizability of the reactant molecule, and μ is the reduced mass] for the reaction of $RhAl_3O_4^+$ with CH_4 is 11.2×10^{-10} cm^3 $molecule^{-1}$ s^{-1}, corresponding to the reaction efficiency ($\phi = k_1/k_{coll}$) of 66%. Similarly, the ϕ value for the reaction of $RhAl_3O_4^+$ with CD_4 was determined to be 43%.

The observation of $RhAl_3O_4CH_2^+$ (+H_2) and $RhAl_3O_3H_4^+$ (+CO) product ions in the reaction of $RhAl_3O_4^+$ with CH_4 suggests generation of syngas. The DFT calculations predicted that the lowest-lying isomer of $RhAl_3O_4^+$ is a doublet and the unpaired spin densities are distributed on the Rh atom which is bonded with one Al and one O atom (Figures 2b and S3). The reaction pathway for syngas formation is shown in Figures 2 and S5. Other pathways tested are shown in Figures S6–S11.

The Rh atom traps methane molecule to form encounter complex I1 with a binding energy of 0.90 eV (Figure 2). The reaction proceeds through the mechanism of oxidative addition (I1 → TS1 → I2), resulting in activation of the first C–H bond and formation of the Rh–CH_3 and Rh–H bonds. After a structural rearrangement (I2 → TS2 → I3), the H atom bonded with Rh transfers to the cluster-support (Al_3O_4) to make an O–H bond (I3 → TS3 → I4), which also results in breaking of the Rh–O bond and formation of a new Rh–Al bond. The intermediate I4 has enough energy (1.65 eV) to activate the second C–H bond (I4 → TS4 → I5) to form the second Rh–H bond. The reaction complex can relax (I5 → I6 → I7) to form a more stable intermediate I7 with a three-membered-ring structure of Al–CH_2–Rh.

To proceed to the remaining part of the reaction, the CH_2 unit in I7 needs to make a chemical bond with an O atom to form a CH_2O moiety (I7 → TS7 → I8). The energy of TS7 is slightly lower than the separated reactants and the absolute energy barrier to overcome TS7 is high (1.82 eV). As a result, in addition to the formation of I8 that eventually generated the syngas, the stabilization of I7 through collisions with bath gas (~1 Pa He) in the reactor was possible, which interprets the observation of the association complex ($RhAl_3O_4CH_4^+$) in Figure 1. The DFT calculations also predicted that I7 can further react with a second CH_4 molecule to form the experimentally observed product $RhAl_3O_3H_2^+$ (I7 + CH_4 → $RhAl_3O_3H_2^+$ + C_2H_5OH). This secondary reaction with interesting C–C coupling process is not the main focus of this study and the mechanism is shown in Figure S11.

As shown in Figure 2, after the formation of CH_2O unit, the activation of the third C–H bond to form the third Rh–H bond can occur (I8 → TS8 → I9). Test calculations (Figure S8) suggested that activation of the third C–H bond before the CH_2O formation is unfavorable. After a structural rearrangement to break the Al–OCH bond in I9 (I9 → TS9 → I10), the fourth C–H bond can be activated and the fourth Rh–H bond is formed (I10 → TS10 → I11). In the intermediate I11, the Rh atom is 6-fold coordinated (with one CO unit, two Al, and

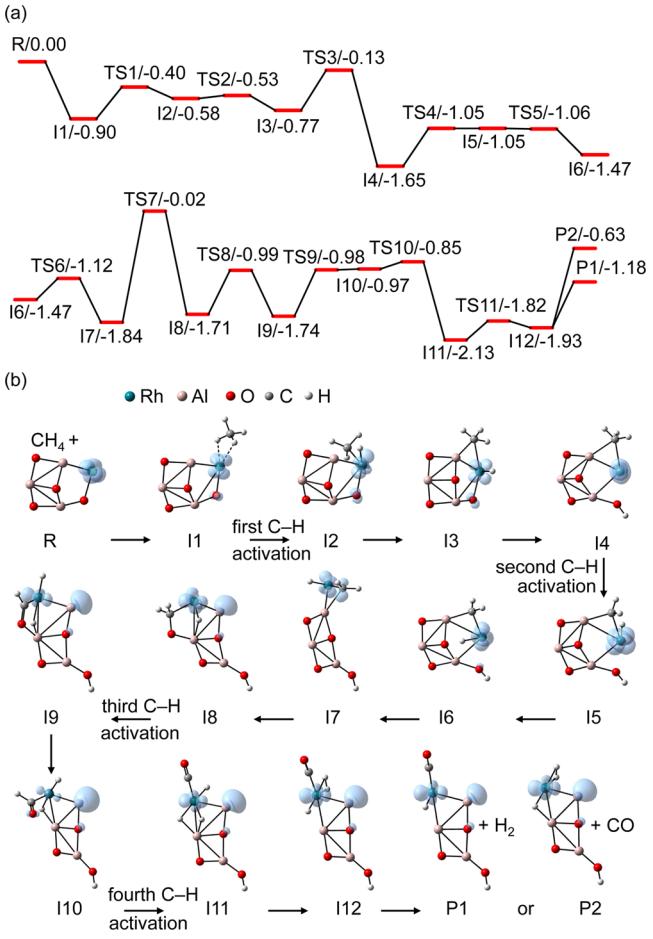

Figure 2. DFT calculated potential energy profile for the reaction channels (1) and (2). The relative energies of reaction intermediates (I1–I12), TSs (TS1–TS11), and products (P1 and P2) with respect to the separated reactants (R, $RhAl_3O_4^+$ + CH_4) are given in eV. Profiles for unpaired spin densities are shown. The structures of R, I1–I12, P1, and P2 are plotted and those of TS1–TS11 can be found in the Supporting Information.

three H atoms). Two of the three H atoms on Rh can make a H_2 unit (I11 → TS11 → I12). Finally, the H_2 and CO molecules can be evaporated from Rh of I12 to form product ions $RhAl_3O_4CH_2^+$ and $RhAl_3O_3H_4^+$, respectively. All of the reaction intermediates and TSs shown in Figure 2 are lower in energy than the separated reactants so the gas-phase reaction channels (1) and (2) are thermodynamically and kinetically favorable. It is noteworthy that the formation of H_2 after activation of only two C–H bonds has also been tested (Figure S9) while such a process is thermodynamically unfavorable.

The DFT calculated energy of P1 (−1.18 eV) is lower than that of P2 (−0.63 eV) by 0.55 eV so the generation of P1 is more favorable than that of P2 in terms of thermodynamics. Based on the DFT determined energetics, the VTST calculations (Table S2 and Figure S13) predicted that the I11 dissociates to P1 ($RhAl_3O_4CH_2^+$ + H_2) and P2 ($RhAl_3O_3H_4^+$ + CO) with the rates of 3.7×10^{11} and 5.4×10^8 s^{-1}, respectively. The relative VTST rate constants are qualitatively consistent with the observation (Figure 1b) that $RhAl_3O_4CH_2^+$ signal was more intense than $RhAl_3O_3H_4^+$ in the experiment. However, the VTST result suggested that the intensity of $RhAl_3O_4CH_2^+$ can be stronger than that of $RhAl_3O_3H_4^+$ by a factor of about 685 rather than the experimentally observed intensity ratio of

DOI: 10.1021/jacs.6b05454
J. Am. Chem. Soc. 2016, 138, 12854–12860

3.4 (Figure 1b). This can be due to the computational errors of the adopted DFT functional. The more reliable RCCSD(T) method predicted that the relative energies of P1 and P2 are −0.81 and −0.50 eV, respectively. In this case, the VTST rates for the dissociations of I11 to P1 and P2 are 1.0×10^8 and 1.7×10^6 s^{-1}, respectively, which better (685 → 59) agrees with the experimental intensity ratio (3.4) of $RhAl_3O_4CH_2^+$ to $RhAl_3O_3H_4^+$ (Figure 1b). As a result, the relative energies can be over- or underestimated by around 0.1−0.4 eV with the B3P86 functional.

The experimental reaction efficiencies of $RhAl_3O_4^+$ with CH_4 and CD_4 are 66% and 43%, respectively. It means that a fair amount of the encounter complex (I1, 34% of $RhAl_3O_4CH_4^+$ and 57% of $RhAl_3O_4CD_4^+$) can dissociate back to the separated reactants. The rates of the back dissociation (I1 → R) and forward conversion (I1 → TS3) were calculated (Figure S13 and Table S3) and the results indicated that the DFT energy of TS3 was overestimated by around 0.17 eV. If the energy of TS3 could be lowered down to −0.30 eV, the reaction efficiencies of $RhAl_3O_4^+ + CH_4$ and $RhAl_3O_4^+ + CD_4$ were calculated to be 66% and 29%, respectively. The more efficient reaction with CH_4 than that with CD_4 was correctly predicted. The poor match of the reaction efficiency for $RhAl_3O_4^+ + CD_4$ (29% by calculation vs 43% by experiment) could be due to various approximations (such as harmonic vibrations) used in the RRKM and VTST calculations.[17]

The RRKM theory (Table S4) was also used to calculate the rate to overcome the highest barrier (I7 → TS7) in Figure 2. Based on the DFT energies, the calculated rate (1.1×10^{-2} s^{-1}) for the CH_4 reaction system is too slow compared with the rate (2.9×10^5 s^{-1}) of collisions between the cluster ions and the bath gas He. It means that almost all of the product ions would be the association complex $RhAl_3O_4CH_4^+$. However, as shown in Figure 1b, about 51% $RhAl_3O_4CH_4^+$ ions were converted to separated products. The DFT calculations could overestimate the energy of TS7 and the barrier of process I7 → TS7. The energies of I7 and TS7 might be adjusted (by 0.3−0.4 eV) so that the rate of internal conversion (I7 → TS7) could catch the collisional rate. In this case, the RRKM rate of process I7 → TS7 for $RhAl_3O_4CH_4^+$ is larger than that for $RhAl_3O_4CD_4^+$ by a factor of 1.9 (Table S4) although the process I7 → TS7 involves formation of the C−O bond rather than activation of the C−H bond. This can be due to the fact that the deuterium system has denser vibrational states and the intracluster vibrational energy redistribution to successfully overcome a given energy barrier should be slower. As a result, the deuterium system has more chance to be stabilized through the collisions with the He bath gas, which is consistent with the experimental results of Figure 1b and d: 51% $RhAl_3O_4CH_4^+$ ions were converted to separated products while the corresponding value is only 22% for the deuterium reaction system ($RhAl_3O_4CD_4^+$).

The reactions between metal oxide clusters and methane have been extensively studied. Most of the reactive systems free of noble metal (NM) atoms activate methane through oxygen centered radicals ($O^{-\bullet}$) with the mechanism of hydrogen atom abstraction ($O^{-\bullet} + CH_4 \rightarrow OH^- + CH_3^\bullet$) that involves the activation of only one C−H bond.[6a,22,23] Recently, it has been found that doping NM atoms of gold[24] and platinum[25] to metal oxide clusters containing the $O^{-\bullet}$ radicals can trigger novel reactions such as the activations of two C−H bonds of a CH_4 molecule to form the formaldehyde molecule. The Au atom in $AuNbO_3^+$ cluster promotes methane transformation after the activation of the first C−H bond by the $O^{-\bullet}$ radical.[24] The Pt atom in $PtAl_2O_4^-$ cluster with the $O^{-\bullet}$ radical functions as the active site to cleave two C−H bonds of a methane molecule.[25] In this study, the computational results indicated that there is no $O^{-\bullet}$ radical in $RhAl_3O_4^+$ cluster and all of the spin densities are distributed on the Rh atom. As the coordination number of Rh increases, some of the spin densities transfer to the Al atom bonded with the Rh atom (Figure 2). Furthermore, we have identified that the cluster doped with NM of Rh exhibits unique reactivity: the Rh atom in $RhAl_3O_4^+$ can cleave all of the four C−H bonds of a methane molecule to produce syngas.

In addition to the unique performance of Rh atom, the cluster-support (Al_3O_4) also plays important roles in methane conversion to syngas: (1) the Al_3O_4 unit accepts the first H atom delivered by Rh atom from CH_4 to form the O−H bond (I3 → I4 in Figure 2), the process of which releases additional energy (0.88 eV) to facilitate the subsequent chemical transformation; (2) two of the three H atoms bonded with Rh atom in I11 are also bonded with Al atom and the formations of the Al−H bonds help to stabilize the reaction intermediates including I8−I10; and (3) the Al_3O_4 unit provides an O atom so that CH_4 can be converted to CO.

To further study the property and activity of Rh atom in methane conversion to syngas, the natural bond orbital (NBO) analysis was conducted (Figures 3 and S14). It has been

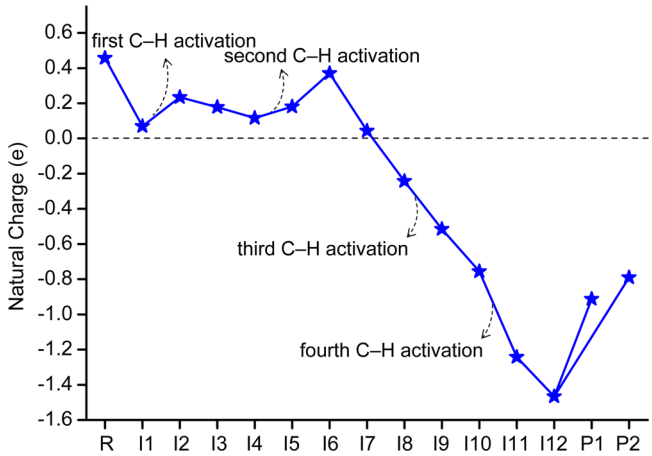

Figure 3. DFT calculated natural charges (e) on the Rh atom.

reported that the bare neutral Rh atom can activate one C−H bond of methane under matrix isolation conditions.[8a] In the reaction of $RhAl_3O_4^+$ with methane, the nearly neutral Rh (0.07 e) in the intermediate I1 retains the reactivity of bare Rh atom to cleave the first C−H bond of CH_4, the process of which is the crucial step to transform methane. As shown in Figure 3, during the reaction of $RhAl_3O_4^+$ with CH_4, the Rh atom can switch its oxidation states from cationic (R) to nearly neutral (I1) and from neutral to cationic (I1 → I6). The cationic Rh can switch to anionic Rh after forming the CH_2−O bond (I7 → I8). During the oxidation of CH_2O to CO, the Rh atom, rather than O atom(s), acts as the oxidant to accept the electrons. The Rh atom becomes very negatively charged (−1.47 e) in I12. The appearance of anionic Rh has been proposed in condensed-phase studies while there was little information on its performance on the chemical reactions.[26] This study has demonstrated that the anionic Rh plays a dominant role in the activation of C−H bonds of the formaldehyde moiety to produce CO. The previous studies reported that Au atom can

DOI: 10.1021/jacs.6b05454
J. Am. Chem. Soc. 2016, 138, 12854−12860

accept negative charges of about −1 e in the reactions with small molecules.[24,27] In the reaction of $RhAl_3O_4^+$ with CH_4, the negative charges of about −2 e can be accepted by the Rh atom (Rh carries 0.46 e in R and −1.47 e in I12). Such a high electron-withdrawing capability of Rh atom tends to be a strong driving force to transform CH_4 to CO and H_2 in this study.

The activation of the first C−H bond of methane by the aluminum site has also been calculated and a higher barrier (−0.08 eV) by Al than that (−0.13 eV) by Rh was predicted (Figure S7). This suggests that the Rh atom plays an important role in methane activation. To further demonstrate that methane activation and conversion to syngas in the reaction between the $RhAl_3O_4^+$ cluster and CH_4 is due to the unique properties of rhodium atom, the reactivity of the Rh-free metal oxide cluster $Al_4O_4^+$ was considered experimentally and theoretically (Figures S2, S4, and S12). Upon the interaction of $Al_4O_4^+$ with CH_4, no transformation product peak was observed except a weak peak due to the CH_4 adsorption. Furthermore, the computational results also indicated that the first C−H bond of methane cannot be activated by the $Al_4O_4^+$ cluster under thermal collision conditions. Doped clusters in the gas-phase often exert dramatic effects on the reactions with small molecules.[6b] For example, in the reaction of methane with the $Al_2O_3^+$ cluster, two reaction channels, hydrogen atom transfer (HAT) and formaldehyde elimination were observed.[9a] In contrast, only the HAT channel was observed when one aluminum atom in $Al_2O_3^+$ was substituted by an yttrium atom.[22k] In this study, replacing one aluminum atom of the $Al_4O_4^+$ cluster by a rhodium atom to form the $RhAl_3O_4^+$ cluster has resulted in highly enhanced reactivity leading to the generation of syngas from methane.

In condensed-phase studies, the syngas was observed upon the interaction of methane with Rh nanoparticles supported on Al_2O_3 in the absence of any oxygen source.[3b] The condensed-phase result well parallels the result of the gas-phase reaction between the $RhAl_3O_4^+$ cluster and CH_4. Two possibilities for CO formation were proposed for condensed-phase reactions. The first one involves the dissociation of gas-phase CH_4 on metallic Rh sites to CH_x and H species. The H species can be oxidized to H_2O by lattice oxygen of Al_2O_3 at the interface between the Rh nanoparticles and the support. The formed H_2O molecules oxidize the remaining surface CH_x fragments to CO. The second one involves direct oxidation of the surface CH_x species to CO by the lattice oxygen of Al_2O_3. The second mechanism of CO formation on Rh/Al_2O_3 catalysts well parallels similar behavior of the reaction between the $RhAl_3O_4^+$ cluster and CH_4. Therefore, this work reveals a molecular level origin for the condensed-phase experimental observations that trace amounts of Rh can promote the direct participation of lattice oxygen of chemically very inert supports such as aluminum oxide (Al_2O_3) to oxidize methane to carbon monoxide.[3b,c,5]

The oxidative reforming of methane to syngas on typical Rh/Al_2O_3 catalysts may be divided into two steps:[3b,d,4b] (1) the oxidation of methane by Rh/Al_2O_3 and the simultaneous formation of the reduced catalyst, and (2) the oxidation of the reduced Rh/Al_2O_3 by the oxidizers such as H_2O and CO_2.

$$RhAl_3O_3H_2^+ + H_2O \rightarrow RhAl_3O_4^+ + 2H_2 \quad \Delta H_0 = 2.25 \text{ eV} \tag{3}$$

$$RhAl_3O_3H_2^+ + CO_2 \rightarrow RhAl_3O_4^+ + H_2 + CO \quad \Delta H_0 = 3.01 \text{ eV} \tag{4}$$

As shown in reactions 3 and 4, the theoretical calculations predicted that the O refilling by H_2O or CO_2 in the cluster system is endothermic. This prediction is consistent with the condensed-phase result that in addition to the CH_4 activation, the activation of H_2O or CO_2 to refill the O atom is also very important to close the catalytic cycle. For example, the dissociation of CO_2 to CO and O is the rate-determining step in the catalytic reforming of methane to syngas.[3e,f,28] Thus, it will be very important to study the reactivity of the product ions from the cluster ion reactions with methane in the future. The gas-phase catalytic cycles can then be constructed for CH_4 transformation.[29]

4. CONCLUSION

Thermal conversion of methane to syngas mediated by a heteronuclear metal oxide cluster ($RhAl_3O_4^+$) has been identified for the first time by using mass spectrometry and quantum chemistry calculations. The rhodium atom of the $RhAl_3O_4^+$ cluster functions as the active center to cleave all of the four C−H bonds of a CH_4 molecule. The cluster-support (Al_3O_4) accepts the H atoms delivered through Rh atom to release additional energy and provides lattice oxygen to oxidize CH_4 to CO. In this work, the conversion of methane to syngas is driven by the high electron-withdrawing capability of Rh atom that can switch its polarity of oxidation state from positive to negative. Furthermore, this study reveals the molecular level origin for the condensed-phase experimental observation that trace amounts of Rh can promote the direct participation of lattice oxygen of chemically very inert support (Al_2O_3) to oxidize methane to carbon monoxide.

■ ASSOCIATED CONTENT

Supporting Information

The Supporting Information is available free of charge on the ACS Publications website at DOI: 10.1021/jacs.6b05454.

Details of additional theoretical methods and additional experimental and theoretical results (mass spectra, DFT calculated structures and reaction mechanisms, and RRKM rates of conversion) (PDF)

■ AUTHOR INFORMATION

Corresponding Authors

*chemzyx@iccas.ac.cn
*chenh@iccas.ac.cn
*shengguihe@iccas.ac.cn

Notes

The authors declare no competing financial interest.

■ ACKNOWLEDGMENTS

This work was supported by the National Natural Science Foundation of China (Nos. 21325314, 21273247, 21573247, 21290194, and 21521062), the Strategic Priority Research Program of the Chinese Academy of Sciences (XDA09030101).

■ REFERENCES

(1) (a) Verma, D.; Singla, A.; Lal, B.; Sarma, P. M. *Curr. Sci.* **2016**, *110*, 329. (b) Xiong, H.-F.; Jewell, L. L.; Coville, N. J. *ACS Catal.* **2015**, *5*, 2640. (c) Dry, M. E. *Catal. Today* **2002**, *71*, 227. (d) Wender,

DOI: 10.1021/jacs.6b05454
J. Am. Chem. Soc. 2016, 138, 12854−12860

I. *Fuel Process. Technol.* **1996**, *48*, 189. (e) Nguyen, V. N.; Blum, L. *Chem. Ing. Tech.* **2015**, *87*, 354.
(2) (a) Pakhare, D.; Spivey, J. *Chem. Soc. Rev.* **2014**, *43*, 7813. (b) Choudhary, T. V.; Choudhary, V. R. *Angew. Chem., Int. Ed.* **2008**, *47*, 1828.
(3) (a) Kuznetsov, V. V.; Vitovskii, O. V.; Gasenko, O. A. *Theor. Found. Chem. Eng.* **2014**, *48*, 376. (b) Kondratenko, V. A.; Berger-Karin, C.; Kondratenko, E. V. *ACS Catal.* **2014**, *4*, 3136. (c) Berger-Karin, C.; Radnik, J.; Kondratenko, E. V. *J. Catal.* **2011**, *280*, 116. (d) Bitter, J. H.; Seshan, K.; Lercher, J. A. *J. Catal.* **1998**, *176*, 93. (e) Nakamura, J.; Aikawa, K.; Sato, K.; Uchijima, T. *Catal. Lett.* **1994**, *25*, 265. (f) Mark, M. F.; Maier, W. F. *Angew. Chem., Int. Ed. Engl.* **1994**, *33*, 1657. (g) Ashcroft, A. T.; Cheetham, A. K.; Green, M. L. H.; Vernon, P. D. F. *Nature* **1991**, *352*, 225.
(4) (a) Nematollahi, B.; Rezaei, M.; Asghari, M.; Fazeli, A.; Lay, E. N.; Nematollahi, F. *Fuel* **2014**, *134*, 565. (b) Wei, J. M.; Iglesia, E. *J. Catal.* **2004**, *225*, 116.
(5) (a) Berger-Karin, C.; Wohlrab, S.; Rodemerck, U.; Kondratenko, E. V. *Catal. Commun.* **2012**, *18*, 121. (b) Berger-Karin, C.; Sebek, M.; Pohl, M. M.; Bentrup, U.; Kondratenko, V. A.; Steinfeldt, N.; Kondratenko, E. V. *ChemCatChem* **2012**, *4*, 1368.
(6) (a) Ding, X.-L.; Wu, X.-N.; Zhao, Y.-X.; He, S.-G. *Acc. Chem. Res.* **2012**, *45*, 382. (b) Schwarz, H. *Angew. Chem., Int. Ed.* **2015**, *54*, 10090. (c) Jena, P.; Castleman, A. W. *Int. J. Mass Spectrom.* **2015**, *377*, 235. (d) Bernstein, E. R. *Int. J. Mass Spectrom.* **2015**, *377*, 248. (e) Yin, S.; Bernstein, E. R. *Int. J. Mass Spectrom.* **2012**, *321*, 49. (f) Shayeghi, A.; Johnston, R. L.; Rayner, D. M.; Schafer, R.; Fielicke, A. *Angew. Chem., Int. Ed.* **2015**, *54*, 10675. (g) Hermes, A. C.; Hamilton, S. M.; Hopkins, W. S.; Harding, D. J.; Kerpal, C.; Meijer, G.; Fielicke, A.; Mackenzie, S. R. *J. Phys. Chem. Lett.* **2011**, *2*, 3053. (h) Wang, G.-J.; Zhou, M.-F.; Goettel, J. T.; Schrobilgen, G. J.; Su, J.; Li, J.; Schloder, T.; Riedel, S. *Nature* **2014**, *514*, 475. (i) Gong, Y.; Zhou, M.-F.; Andrews, L. *Chem. Rev.* **2009**, *109*, 6765.
(7) (a) Yang, M.-Y.; Yang, H.-Q.; Gao, C.; Qin, S.; Hu, C.-W. *Struct. Chem.* **2011**, *22*, 983. (b) Gao, C.; Yang, H.-Q.; Xu, J.; Qin, S.; Hu, C.-W. *J. Comput. Chem.* **2009**, *31*, 938. (c) Au, C. T.; Liao, M. S.; Ng, C. F. *Chem. Phys. Lett.* **1997**, *267*, 44.
(8) (a) Wang, G.-J.; Chen, M.-H.; Zhou, M.-F. *Chem. Phys. Lett.* **2005**, *412*, 46. (b) Koszinowski, K.; Schlangen, M.; Schröder, D.; Schwarz, H. *Int. J. Mass Spectrom.* **2004**, *237*, 19. (c) Albert, G.; Berg, C.; Beyer, M.; Achatz, U.; Joos, S.; NiednerSchatteburg, G.; Bondybey, V. E. *Chem. Phys. Lett.* **1997**, *268*, 235. (d) Chen, Y. M.; Armentrout, P. B. *J. Phys. Chem.* **1995**, *99*, 10775. (e) Liu, Y.-Y.; Geng, Z.-Y.; Wang, Y.-C.; Liu, J.-L.; Hou, X.-F. *Comput. Theor. Chem.* **2013**, *1015*, 52. (f) Westerberg, J.; Blomberg, M. R. A. *J. Phys. Chem. A* **1998**, *102*, 7303.
(9) (a) Wang, Z.-C.; Dietl, N.; Kretschmer, R.; Ma, J.-B.; Weiske, T.; Schlangen, M.; Schwarz, H. *Angew. Chem., Int. Ed.* **2012**, *51*, 3703. (b) Wang, Z.-C.; Weiske, T.; Kretschmer, R.; Schlangen, M.; Kaupp, M.; Schwarz, H. *J. Am. Chem. Soc.* **2011**, *133*, 16930. (c) Feyel, S.; Döbler, J.; Hoeckendorf, R.; Beyer, M. K.; Sauer, J.; Schwarz, H. *Angew. Chem., Int. Ed.* **2008**, *47*, 1946.
(10) (a) Yuan, Z.; Li, Z.-Y.; Zhou, Z.-X.; Liu, Q.-Y.; Zhao, Y.-X.; He, S.-G. *J. Phys. Chem. C* **2014**, *118*, 14967. (b) Yuan, Z.; Zhao, Y.-X.; Li, X.-N.; He, S.-G. *Int. J. Mass Spectrom.* **2013**, *354*−*355*, 105. (c) Wu, X.-N.; Xu, B.; Meng, J.-H.; He, S.-G. *Int. J. Mass Spectrom.* **2012**, *310*, 57.
(11) Frisch, M. J.; Trucks, G. W.; Schlegel, H. B.; Scuseria, G. E.; Robb, M. A.; Cheeseman, J. R.; Scalmani, G.; Barone, V.; Mennucci, B.; Petersson, G. A.; Nakatsuji, H.; Caricato, M.; Li, X.; Hratchian, H. P.; Izmaylov, A. F.; Bloino, J.; Zheng, G.; Sonnenberg, J. L.; Hada, M.; Ehara, M.; Toyota, K.; Fukuda, R.; Hasegawa, J.; Ishida, M.; Nakajima, T.; Honda, Y.; Kitao, O.; Nakai, H.; Vreven, T.; Montgomery, A. M., Jr.; Peralta, J. E.; Ogliaro, F.; Bearpark, M.; Heyd, J. J.; Brothers, E.; Kudin, K. N.; Staroverov, V. N.; Kobayashi, R.; Normand, J.; Raghavachari, K.; Rendell, A.; Burant, J. C.; Iyengar, S. S.; Tomasi, J.; Cossi, M.; Rega, N.; Millam, J. M.; Klene, M.; Knox, J. E.; Cross, J. B.; Bakken, V.; Adamo, C.; Jaramillo, J.; Gomperts, R.; Stratmann, R. E.; Yazyev, O.; Austin, A. J.; Cammi, R.; Pomelli, C.; Ochterski, J. W.; Martin, R. L.; Morokuma, K.; Zakrzewski, V. G.; Voth, G. A.; Salvador, P.; Dannenberg, J. J.; Dapprich, S.; Daniels, A. D.; Farkas, Ö.; Foresman, J. B.; Ortiz, J. V.; Cioslowski, J.; Fox, D. J. *Gaussian09*; Gaussian, Inc.: Wallingford, CT, 2009.
(12) (a) Becke, A. D. *J. Chem. Phys.* **1993**, *98*, 5648. (b) Perdew, J. P. *Phys. Rev. B: Condens. Matter Mater. Phys.* **1986**, *33*, 8822.
(13) Berente, I.; Naray-Szabo, G. *J. Phys. Chem. A* **2006**, *110*, 772.
(14) (a) Gonzalez, C.; Schlegel, H. B. *J. Chem. Phys.* **1989**, *90*, 2154. (b) Gonzalez, C.; Schlegel, H. B. *J. Phys. Chem.* **1990**, *94*, 5523.
(15) Glendening, E. D.; Reed, A. E.; Carpenter, J. E.; Weinhold, F. *NBO 3.1*; Theoretical Chemistry Institute, University of Wisconsin: Madison, WI, 1996.
(16) Werner, H.-J.; Knowles, P. J.; Lindh, R.; Manby, F. R.; Schütz, M.; Celani, P.; Korona, T.; Mitrushenkov, A.; Rauhut, G.; Adler, T. B.; Amos, R. D.; Bernhardsson, A.; Berning, A.; Cooper, D. L.; Deegan, M. J. O.; Dobbyn, A. J.; Eckert, F.; Goll, E.; Hampel, C.; Hetzer, G.; Hrenar, T.; Knizia, G.; Köppl, C.; Liu, Y.; Lloyd, A. W.; Mata, R. A.; May, A. J.; McNicholas, S. J.; Meyer, W.; Mura, M. E.; Nicklass, A.; Palmieri, P.; Pflüger, K.; Pitzer, R.; Reiher, M.; Schumann, U.; Stoll, H.; Stone, A. J.; Tarroni, R.; Thorsteinsson, T.; Wang, M.; Wolf, A. *MOLPRO, version 2010.1, a package of ab initio programs*. See http://www.molpro.net.
(17) Steinfeld, J. I.; Francisco, J. S.; Hase, W. L. *Chemical Kinetics and Dynamics*; Prentice-Hall: Upper Saddle River, NJ, 1999; p 231 and 313.
(18) Beyer, T.; Swinehart, D. F. *Commun. ACM* **1973**, *16*, 379.
(19) (a) Li, S.; Mirabal, A.; Demuth, J.; Wöste, L.; Siebert, T. *J. Am. Chem. Soc.* **2008**, *130*, 16832. (b) Li, S.; Demuth, J.; Mirabal, A.; Wöste, L.; Siebert, T. *Phys. Chem. Chem. Phys.* **2012**, *14*, 148.
(20) Meng, J.-H.; He, S.-G. *J. Phys. Chem. Lett.* **2014**, *5*, 3890.
(21) (a) Kummerlöwe, G.; Beyer, M. K. *Int. J. Mass Spectrom.* **2005**, *244*, 84. (b) Gioumousis, G.; Stevenson, D. P. *J. Chem. Phys.* **1958**, *29*, 294.
(22) (a) Schwarz, H. *Chem. Phys. Lett.* **2015**, *629*, 91. (b) Dietl, N.; Schlangen, M.; Schwarz, H. *Angew. Chem., Int. Ed.* **2012**, *51*, 5544. (c) Zhao, Y.-X.; Wu, X.-N.; Ma, J.-B.; He, S.-G.; Ding, X.-L. *Phys. Chem. Chem. Phys.* **2011**, *13*, 1925. (d) Li, J.; Wu, X.-N.; Schlangen, M.; Zhou, S.; Gonzalez-Navarrete, P.; Tang, S.; Schwarz, H. *Angew. Chem., Int. Ed.* **2015**, *54*, 5074. (e) Li, J.; Wu, X.-N.; Zhou, S.-D.; Tang, S.-Y.; Schlangen, M.; Schwarz, H. *Angew. Chem., Int. Ed.* **2015**, *54*, 12298. (f) Wu, X.-N.; Ding, X.-L.; Li, Z.-Y.; Zhao, Y.-X.; He, S.-G. *J. Phys. Chem. C* **2014**, *118*, 24062. (g) Meng, J.-H.; Deng, X.-J.; Li, Z.-Y.; He, S.-G.; Zheng, W.-J. *Chem. - Eur. J.* **2014**, *20*, 5580. (h) Meng, J.-H.; Zhao, Y.-X.; He, S.-G. *J. Phys. Chem. C* **2013**, *117*, 17548. (i) Wang, Z. C.; Liu, J. W.; Schlangen, M.; Weiske, T.; Schröder, D.; Sauer, J.; Schwarz, H. *Chem. - Eur. J.* **2013**, *19*, 11496. (j) Li, Z.-Y.; Zhao, Y.-X.; Wu, X.-N.; Ding, X.-L.; He, S.-G. *Chem. - Eur. J.* **2011**, *17*, 11728. (k) Ma, J.-B.; Wang, Z.-C.; Schlangen, M.; He, S.-G.; Schwarz, H. *Angew. Chem., Int. Ed.* **2012**, *51*, 5991.
(23) (a) Beyer, M. K.; Berg, C. B.; Bondybey, V. E. *Phys. Chem. Chem. Phys.* **2001**, *3*, 1840. (b) Kretschmer, R.; Schlangen, M.; Schwarz, H. *Angew. Chem., Int. Ed.* **2013**, *52*, 6097.
(24) (a) Wang, L.-N.; Zhou, Z.-X.; Li, X.-N.; Ma, T.-M.; He, S.-G. *Chem. - Eur. J.* **2015**, *21*, 6957. (b) Wu, X.-N.; Li, X.-N.; Ding, X.-L.; He, S.-G. *Angew. Chem., Int. Ed.* **2013**, *52*, 2444.
(25) Zhao, Y.-X.; Li, Z.-Y.; Yuan, Z.; Li, X.-N.; He, S.-G. *Angew. Chem., Int. Ed.* **2014**, *53*, 9482.
(26) (a) Ševčíková, K.; Kolářová, T.; Skála, T.; Tsud, N.; Václavů, M.; Lykhach, Y.; Matolín, V.; Nehasil, V. *Appl. Surf. Sci.* **2015**, *332*, 747. (b) Mora, M. A.; Mora-Ramirez, M. A. *J. Mol. Model.* **2014**, *20*, 2299. (c) Kinuta, H.; Takahashi, H.; Tobisu, M.; Mori, S.; Chatani, N. *Bull. Chem. Soc. Jpn.* **2014**, *87*, 655. (d) Gomez, T.; Florez, E.; Rodriguez, J. A.; Illas, F. *J. Phys. Chem. C* **2010**, *114*, 1622. (e) Zafeiratos, S.; Nehasil, V.; Ladas, S. *Surf. Sci.* **1999**, *433*, 612. (f) Li, X.-N.; Zhang, H.-M.; Yuan, Z.; He, S.-G. *Nat. Commun.* **2016**, *7*, 11404.
(27) (a) Li, Z.-Y.; Yuan, Z.; Li, X.-N.; Zhao, Y.-X.; He, S.-G. *J. Am. Chem. Soc.* **2014**, *136*, 14307. (b) Li, X.-N.; Yuan, Z.; He, S.-G. *J. Am. Chem. Soc.* **2014**, *136*, 3617. (c) Yuan, Z.; Li, X.-N.; He, S.-G. *J. Phys. Chem. Lett.* **2014**, *5*, 1585. (d) Li, Y.-K.; Meng, J.-H.; He, S.-G. *Int. J. Mass Spectrom.* **2015**, *381*−*382*, 10. (e) Li, Z.-Y.; Li, H.-F.; Zhao, Y.-X.;

DOI: 10.1021/jacs.6b05454
J. Am. Chem. Soc. 2016, 138, 12854−12860

He, S.-G. *J. Am. Chem. Soc.* **2016**, *138*, 9437. (f) Zhao, Y.-X.; Li, X.-N.; Yuan, Z.; Liu, Q.-Y.; Shi, Q.; He, S.-G. *Chem. Sci.* **2016**, *7*, 4730.
(28) (a) Hei, M.-J.; Chen, H.-B.; Yi, J.; Liao, D.-W. *Surf. Sci.* **1998**, *417*, 82. (b) Rostrup-Nielsen, J. R.; Bak Hansen, J. H. *J. Catal.* **1993**, *144*, 38.
(29) (a) Lang, S. M.; Bernhardt, T. M.; Barnett, R. N.; Landman, U. *Angew. Chem., Int. Ed.* **2010**, *49*, 980. (b) Wesendrup, R.; Schröder, D.; Schwarz, H. *Angew. Chem., Int. Ed. Engl.* **1994**, *33*, 1174.

DOI: 10.1021/jacs.6b05454
J. Am. Chem. Soc. 2016, 138, 12854−12860